PERGAMON

Journal of Structural Geology 24 (2002) 1179–1193

JOURNAL OF STRUCTURAL GEOLOGY

www.elsevier.com/locate/jstrugeo

Dissolution and replacement creep: a significant deformation mechanism in mid-crustal rocks

R.P. Wintsch[a,*], Keewook Yi[a,b]

[a]*Department of Geological Sciences, Indiana University, Bloomington, IN 47405, USA*
[b]*School of Earth and Environmental Sciences, Seoul National University, Seoul, South Korea*

Received 4 December 2000; revised 2 June 2001; accepted 26 June 2001

Abstract

Zoning patterns and zoning truncations in metamorphic minerals in a granodioritic orthogneiss indicate that strain and *S–C* fabrics in these rocks were produced by dissolution, precipitation, and replacement processes, even at epidote–amphibolite facies metamorphic conditions. The metamorphic fabric is defined by alternating layers and folia dominated by quartz, feldspars, and biotite + epidote. Zoning patterns in most metamorphic plagioclase, orthoclase, epidote, and sphene are truncated at boundaries normal to the shortening direction, suggesting dissolution. Interfaces of relict igneous orthoclase phenocrysts that face the shortening direction are embayed and replaced by biotite, epidote, and myrmekitic intergrowths of plagioclase and quartz. Metamorphic plagioclase grains are also replaced by epidote. We interpret these microstructures to reflect strain-enhanced dissolution. The cores of many grains show asymmetric overgrowths with at least two generations of beards, all oriented on the ends of grains that face the extension direction. We interpret these textures to reflect precipitation of components dissolved by deformation-enhanced dissolution. While biotite and quartz probably deformed by dislocation creep, the overall deformation was accommodated by dissolution perpendicular to the shortening direction, and precipitation parallel to it. These chemical processes must have been activated at lower stresses than the dislocation creep predicted from extrapolations of data from experiments in dry rocks. Thus wet crust is likely to be weaker than calculated from these experimental studies. © 2002 Elsevier Science Ltd. All rights reserved.

Keywords: Dissolution; Precipitation; Replacement creep; Pressure solution; Metamorphic reaction mechanism

1. Introduction

Evidence from naturally deformed rocks for the operation of solution transfer is now well documented in sedimentary and low-grade metamorphic rocks (e.g. Passchier and Trouw, 1996). Most significantly, the development of cleavage and metamorphic fabric is now identified to be a chemical process, albeit mechanically induced. The differentiation is thought to be caused by the dissolution of quartz and feldspar from developing mica-rich domains, and precipitation into growing quartz–feldspar domains. Bulk chemical analytical studies do not support the proposition that silica is removed from the developing slate at the kilometer scale (e.g. Wright and Platt, 1982). On the contrary, micas and feldspars as well as quartz appear to dissolve and reprecipitate locally (centimeter scale), with only minor and trace elements that are differentially mobile moving >100 m (e.g. Wintsch et al., 1991). The sites of dissolution are the surfaces normal to the principal shortening direction, as has been recognized in sandstones (e.g. Blatt, 1992), metaconglomerates (Mosher, 1976), and augen gneisses (Simpson and Wintsch, 1989), commonly by the concentration of less soluble minerals, 'insoluble residue'. The dissolved components may precipitate as quartz, feldspar, and even monazite, forming beards on host grains (Wintsch and Knipe, 1983; Williams et al., 1999).

In rocks under sufficiently high-grade metamorphic conditions, dislocation glide and climb are activated progressively in phyllosilicates, then in quartz, and finally in feldspars and pyroxenes (Passchier and Trouw, 1996). Thus in dry rocks dislocation creep may be the most important deformation mechanism in the ductile deformation of higher temperature (>300°C), lower crustal rocks (Fig. 1). Where fluids are present, however, a field of dissolution and precipitation displaces the dislocation creep field. This is best documented in low-grade rocks of ~200–300°C and is typically called 'pressure solution' (Fig. 1; Snoke et al., 1998).

In this contribution we describe an orthogneiss metamorphosed to wet epidote–amphibolite facies conditions.

* Corresponding author. Tel.: +1-812-855-4018; fax: +1-812-855-7899.
E-mail address: wintsch@indiana.edu (R.P. Wintsch).

0191-8141/02/$ - see front matter © 2002 Elsevier Science Ltd. All rights reserved.
PII: S0191-8141(01)00100-6

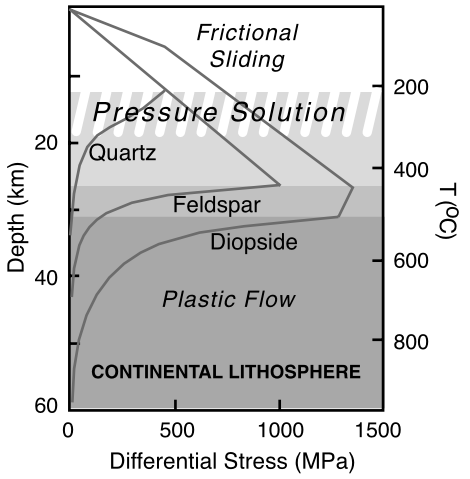

Fig. 1. Diagram showing the strength envelope of rocks in which frictional sliding first in quartz-rich rocks, followed by feldspar-rich and finally by diopside-rich rocks gives way to plastic flow at higher temperatures (compiled from Kohlstedt et al. (1995) and Rybacki and Dresen (2000)). The addition of a 'pressure solution creep' field is from Snoke et al. (1998).

The foliation development, metamorphic differentiation, and grain shape in these rocks are all most easily explained in terms of dissolution, precipitation, and replacement, with relatively little evidence for dislocation creep. If these fluid-dependant deformation mechanisms are representative of processes operating in wet rocks at high grades, then dislocation creep may not be the prevailing deformation mechanism as suggested by the extrapolation of experimental results from dry rocks (see Fig. 1).

2. Geologic setting

The samples analysed in this study were collected in the Glastonbury gneiss in north-central Connecticut (Fig. 2). The Glastonbury gneiss is a complex of Ordovician volcanic and plutonic rocks that comprise the Bronson Hill terrane of central New England. It includes metamorphosed granitic, granodioritic, trondjemitic, and dioritic orthogneisses and schists. U–Pb geochronology on zircon and sphene in this gneiss (Leo et al., 1984; Aleinikoff et al., 2002) and on the Bronson Hill rocks in general (Zartman and Leo, 1985; Tucker and Robinson, 1990) confirm a Late Ordovician igneous crystallization age for these rocks.

Apparently all Bronson Hill rocks were metamorphosed twice. In New Hampshire and Massachusetts, U–Pb geochronology and $^{40}Ar/^{39}Ar$ hornblende thermochronology confirms amphibolite facies metamorphism and cooling from the early Devonian Acadian orogeny. However, Carboniferous to Permian $^{40}Ar/^{39}Ar$ mica and feldspar cooling ages document an Alleghanian greenschist facies metamorphic overprint (Harrison et al., 1989). In Connecticut, the intensity of Alleghanian overprinting is sufficiently high that U–Pb ages of all metamorphic sphene and all $^{40}Ar/^{39}Ar$ hornblende and mica cooling ages yield

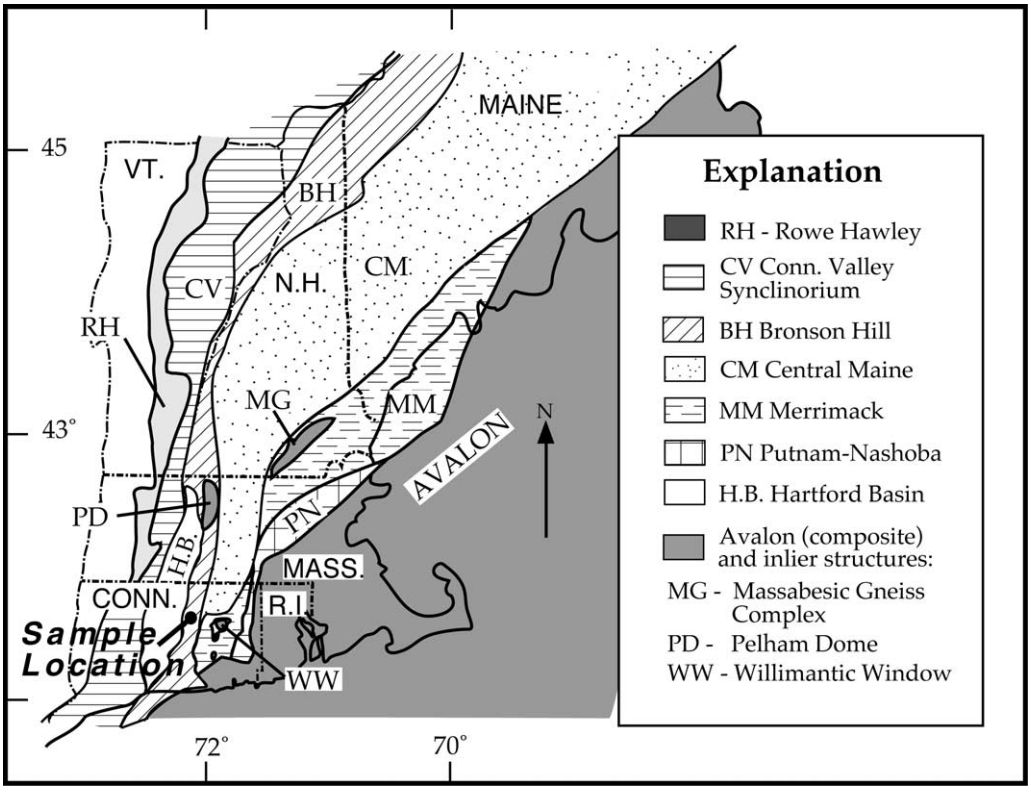

Fig. 2. Map of New England showing the distribution of lithotectonic terranes or zones, and the location of our study area within the Glastonbury gneiss of the Bronson Hill terrane of northern Connecticut.

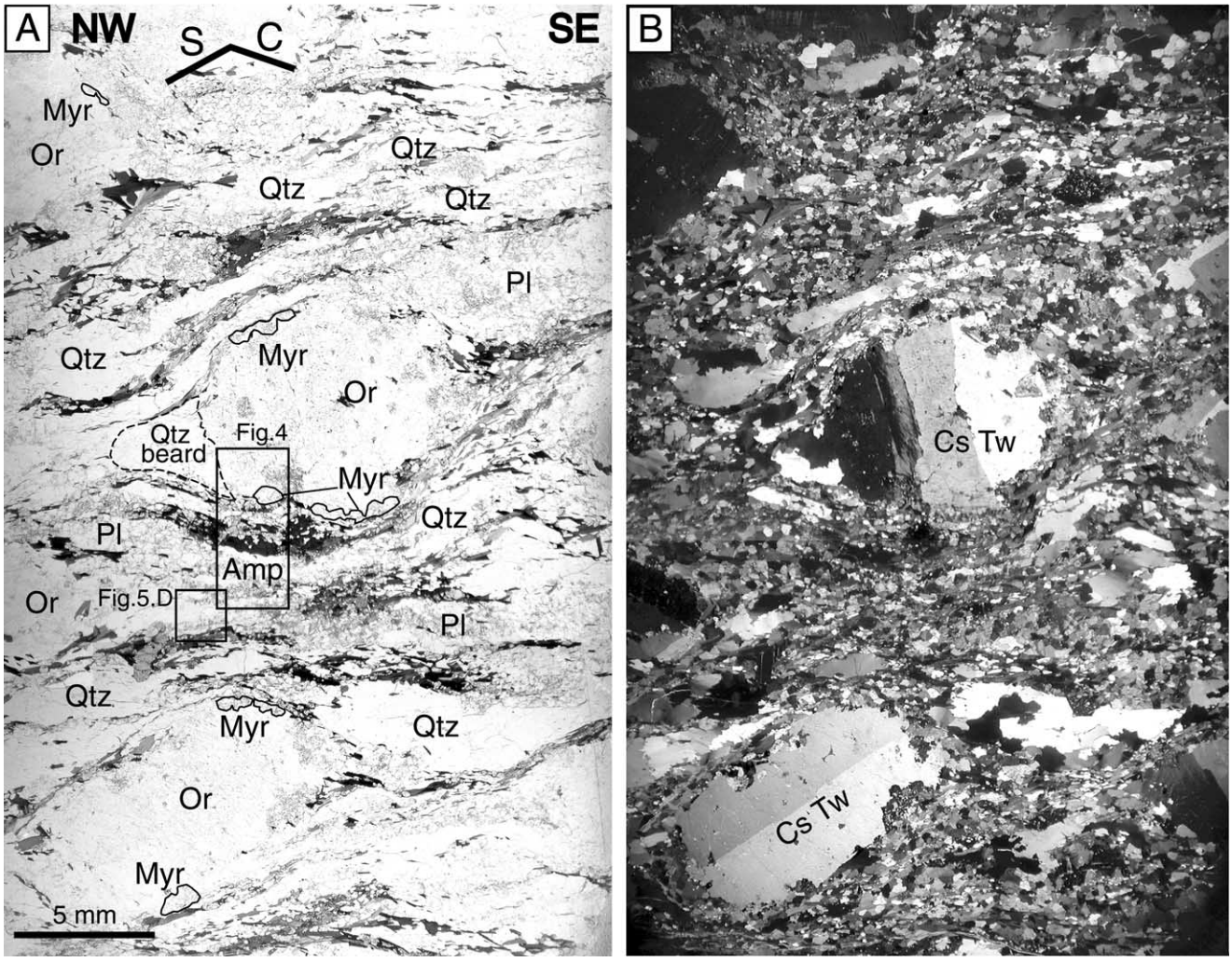

Fig. 3. Plane light and crossed polarized light images of augen gneiss from the Glastonbury Complex. The images show 1 cm diameter grains of orthoclase (Or) with Carlsbad twinning (Cs Tw in B), locally embayed by myrmekite (Myr). Darker layers in A, defined by biotite and epidote layers locally intergrown with amphibole (Amp), outline an *S–C* fabric. These folia are separated by layers of clear quartz (Qtz) and dusty plagioclase (Pl). The locations of Figs. 4 and 5D are indicated.

only Pennsylvanian to Permian ages (Wintsch et al., 1993, 1998; Coleman et al., 1997; Aleinikoff et al., 2002).

3. Observations

The gneisses examined for this study are granodioritic, containing centimeter–diameter K-feldspar crystals in a medium- to coarse-grained matrix of plagioclase, quartz, biotite, epidote, hornblende, K-feldspar, and sphene (Fig. 3). Biotite defines an inconspicuous foliation, and a very conspicuous NNW-plunging lineation parallel to prolate mafic enclaves, such that the rocks are locally *L*-tectonites. *S–C* fabric relationships show that top moved to the SSE (Wintsch et al., 1998). Biotite is the most prominent mineral defining the lineation, but elongate grains of plagioclase, epidote and quartz also define the lineation in their aspect ratios and overgrowth patterns (Figs. 3 and 4). Some of these minerals are Ordovician igneous minerals, and some are metamorphic minerals, produced by metamorphic reactions. Some participate directly in defining the foliation, and some do not. Consequently, each mineral is described separately below.

3.1. Plagioclase

Plagioclase, the most abundant mineral in the gneiss, typically occurs as polygonal untwinned grains 100–300 μm in length (Fig. 4), but some grains may be twice as large (Fig. 5A). It tends to occur in layers and domains from 1 to 5 mm wide and 10–15 mm long where it constitutes >80% of the minerals present (Figs. 3 and 4). Some grains are equant (Fig. 5B and C), but most are elongated parallel to the mineral lineation (Fig. 5A and D). Aspect ratios of 2:1 are typical, but they may be up to 4:1. These grains are universally zoned, with compositions fluctuating

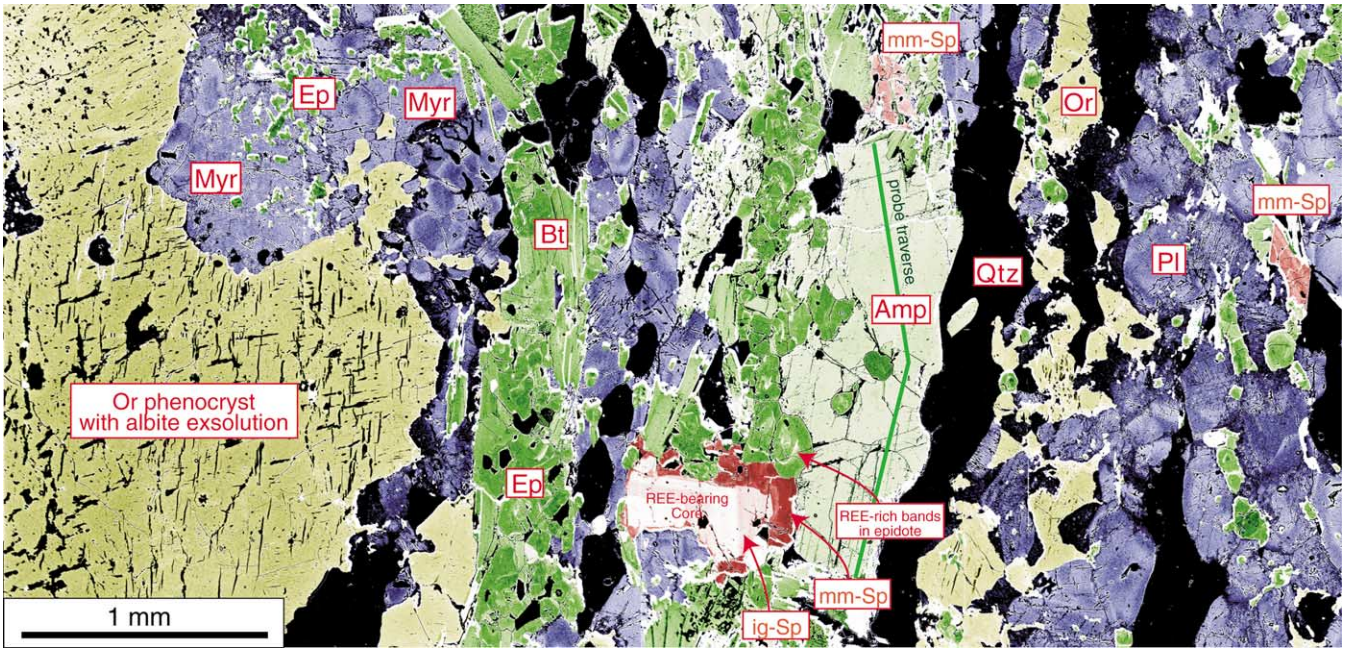

Fig. 4. A colorized backscattered electron image across the foliation shown in Fig. 3. The images were constructed by assembling and separately colorizing four images of the same regions, each adjusted to maximize compositional contrasts in plagioclase (blue), orthoclase (yellow), biotite, epidote, amphibole (green) and sphene (red). The low contrast of quartz and albite (exsolution lamellae in orthoclase only) leave them black. The image shows the strong mineralogical layering parallel to the *C* foliation (Fig. 3). Also visible is compositional zoning in plagioclase (darker blue is more sodic), epidote (pale green is richer in REE), and sphene (pale pinks are richer in REE). The green line identifies the location of the microprobe traverse of Fig. 6C.

between An20 and An30 (Table 1). Zoning patterns define up to three zones. Compositions of core regions are ~An20, surrounded by normally and reversely zoned mantles and finally relatively albitic but still zoned rims (e.g. Fig. 6A). Some grains have rims with an abrupt compositional increase to An30, decaying again to ~An20 or less at the grain boundary. Cores tend to be relatively equant, while mantles, overgrowths and rims with aspect ratios of 6–7 to 1 contribute greatly to the overall elongate shape preferred orientation of the grains (Figs. 4 and 5A–D). Along some grain boundaries, especially along surfaces normal to the inferred extension direction, plagioclase grains are capped by albitic beards (An15, Fig. 6A), which may be associated with epidote (region Ab, Fig. 5D).

3.2. Epidote

Epidote grains are much smaller than plagioclase, from about 50 to 200 μm in diameter, and their shape is variable. Many grains are polygonal and equant, while others are elongated, with aspect ratios up to ~2:1. Many grains are associated with biotite and hornblende (Fig. 4) where they help produce a conspicuous dark layering in the rock (Fig. 3). Other, smaller grains occur with less preferred grain shape orientation, and where included in large plagioclase grains or dispersed in plagioclase-rich domains, they are in near random orientation and show less zoning (Figs. 4 and 5A). Orientation tends to be more strongly aligned parallel to C foliations where epidote is intergrown with biotite (Fig. 5C).

Most epidote grains are zoned, with compositions ranging from pistacite 17 to 25%. Cores tend to be less rich in ferric iron, while rims are richer in pistacite. They may also contain 5–20-μm-wide bands relatively rich in Ce_2O_3 (up to 1.1 wt%), other rare earth elements, and yttrium (Figs. 5E and F and 6B; Table 2). Small grains tend to be zoned, with less pistacitic (Pi 17–20%) cores and more pistacitic (Pi 20–24%) rims. Up to three generations of zoned overgrowths are common in larger grains, their shapes defined by regions of similar pistacite content, and their boundaries outlined by REE-rich bands (e.g. Figs. 5E and 6B).

3.3. Amphibole

Amphibole grains are relatively large, up to 1.5 mm long, with aspect ratios of >3:1. Compositions (Table 3) lie in the magnesiohastingsite field of Leake et al. (1997) when reduced following the scheme of Holland and Blundy (1994) which maximizes the ferric iron estimate. Large grains are weakly zoned, with cores only very slightly enriched in Fe, Al, and Ti (Fig. 6C). They tend to be aligned parallel to the foliation defined by biotite, which is generally associated with it, along with plagioclase and epidote (Fig. 4). Larger grains of magnesiohastingsite are embayed by rounded epidote grains with continuous zoning patterns, suggesting that epidote partially replaces the amphibole.

Magnesiohastingsite grains are commonly in contact with all minerals except orthoclase.

3.4. Biotite

Biotite occurs as subhedral flakes typically 300–600 μm long and 50–300 μm wide. Flakes with aspect ratios of 1:2 to 1:5 are concentrated into folia of subparallel grains that define a conspicuous *S–C* fabric (Fig. 3). Biotite grain contiguity typically exceeds 1–2 cm but is commonly interrupted by subhedral epidote grains. The compositions of biotite grains define a cluster in the iron-rich portion of the phlogopite field (Fig. 6F). Within this cluster grains associated with sphene or epidote are relatively rich in MgO, while those intergrown with quartz and feldspars contain higher concentrations of Al(VI) (Table 3). Most grains are unzoned but some larger grains that extend length-wise from feldspar-dominated domains to sphene-dominated domains show significant zoning in Ti content. This correlation of biotite composition with mineral assemblage reflects the local differences in the activities of FeO and Al_2O_3 defined by these assemblages.

3.5. Sphene

One of the minerals that can be proven to be both igneous and metamorphic is sphene. Grains up to 2 mm long host both igneous cores and metamorphic overgrowths. Ion microprobe analysis and U–Pb dating of these grains (Aleinikoff et al., 2001) show that the core regions are Late Ordovician to Silurian, consistent with zircon U–Pb ages, and thus relict igneous grains. However, the overgrowths are Permian, and therefore Alleghanian and metamorphic in origin. The compositions of the two ages of sphene are distinct. Igneous sphene crystals always contain relatively high REE contents, making them relatively bright in backscattered electron (BSE) images. Metamorphic sphene contains relatively low concentrations of REEs, but much higher Al contents (Table 2), giving it a darker shade of red in Fig. 4.

The structures within these grains, as defined by chemical patterns are also distinctive. Igneous cores show euhedral oscillatory zoning in the concentrations of REEs, as is visible in BSE (lower center, Fig. 4). They also commonly display resorption and overgrowth structures where the overgrowths show anhedral oscillatory zoning (Aleinikoff et al., 2002). These igneous grains universally show anhedral outlines and are overgrown by metamorphic sphene that always isolates the igneous sphene from the matrix mineral assemblage. These rinds range from a few tens up to 100 μm wide, and are themselves zoned, with Al and Nb showing the largest relative percent changes (Wintsch et al., 1999). Subhedral metamorphic sphenes also occur with no igneous cores, and both varieties occur with biotite and epidote (e.g. extreme right, Figs. 4 and 5C). Aspect ratios are commonly >2:1, but regions defined by internal zoning of high and low Nb contents have aspect ratios of >4:1. Zoning patterns in metamorphic sphene show increases in Al from core to rim (Fig. 6D). Concentrations are at a minimum adjacent to the igneous core, and climb (typically with three oscillations) to values near the rims that are almost twice those of igneous grains (Fig. 6D).

3.6. K-feldspar

Orthoclase occurs in several associations. The regional augen structure of the Glastonbury gneiss is defined by pervasive megacrysts of orthoclase about 1 cm in diameter, that universally display Carlsbad twinning. Foliation tends to wrap around these grains, defining the *S–C* fabric (Fig. 3). The sides of the crystals that are subparallel to *S* (i.e. that face the shortening direction) tend to host epidote, biotite, and myrmekitic intergrowths of plagioclase and quartz (Figs. 3 and 5C). Amphibole is universally separated from orthoclase by the above minerals (eg. Fig. 4).

These phenocrysts are strongly perthitic, with albite exsolution lamellae common in all grains (Figs. 4 and 5C; Table 1). Deformation twinning is locally present in some grains, especially adjacent to embayments of myrmekite and epidote. These and locally bent exsolution lamellae suggest local crystal plastic deformation of these grains.

The composition of the orthoclase in these perthites is relatively uniform, about Or94-Ab05-An00-Ce01. However, the integrated bulk composition of the original grain, as determined by averaging the compositions of many broad beam (20 μm) microprobe analyses along long traverses, is ~Or82 (Table 1). BaO is a common minor constituent, with concentrations of ~0.4 wt%, except adjacent to myrmekitic replacements, where the concentration may be three times this amount (Table 1). Two compositions of plagioclase lamellae exist. Fine lamellae (5×50 μm) have a composition of Or02-Ab93-An05, while coarser lamellae with more irregular shapes are less sodic (Table 1). (Recognizing that the analyzed concentrations of Na_2O may be low, we rely more heavily on the K, Ca, and Ba concentrations to define formulae.) The lamellae in most grains are straight but some are curved, defining sigmoidal shapes (Fig. 5C).

A second occurrence of orthoclase is as interstitial grains within a patchwork of plagioclase grains. These grains are not perthitic at the optical or SEM scale, show no twinning or undulosity optically, and are much less sodic than the larger grains (Table 1). They may be polygonal or wedge-shaped (Fig. 3), or they may form crescent-shaped caps or beards on plagioclase or quartz grains (Fig. 5B and D). In all cases, these grains are thickest parallel to the lineation, and taper to zero thickness facing the shortening direction. This geometry is especially common in a third occurrence as beards around orthoclase phenocrysts. Most grains do not display systematic chemical zoning, but some grains that form necks do show U-shaped zoning (Fig. 6E).

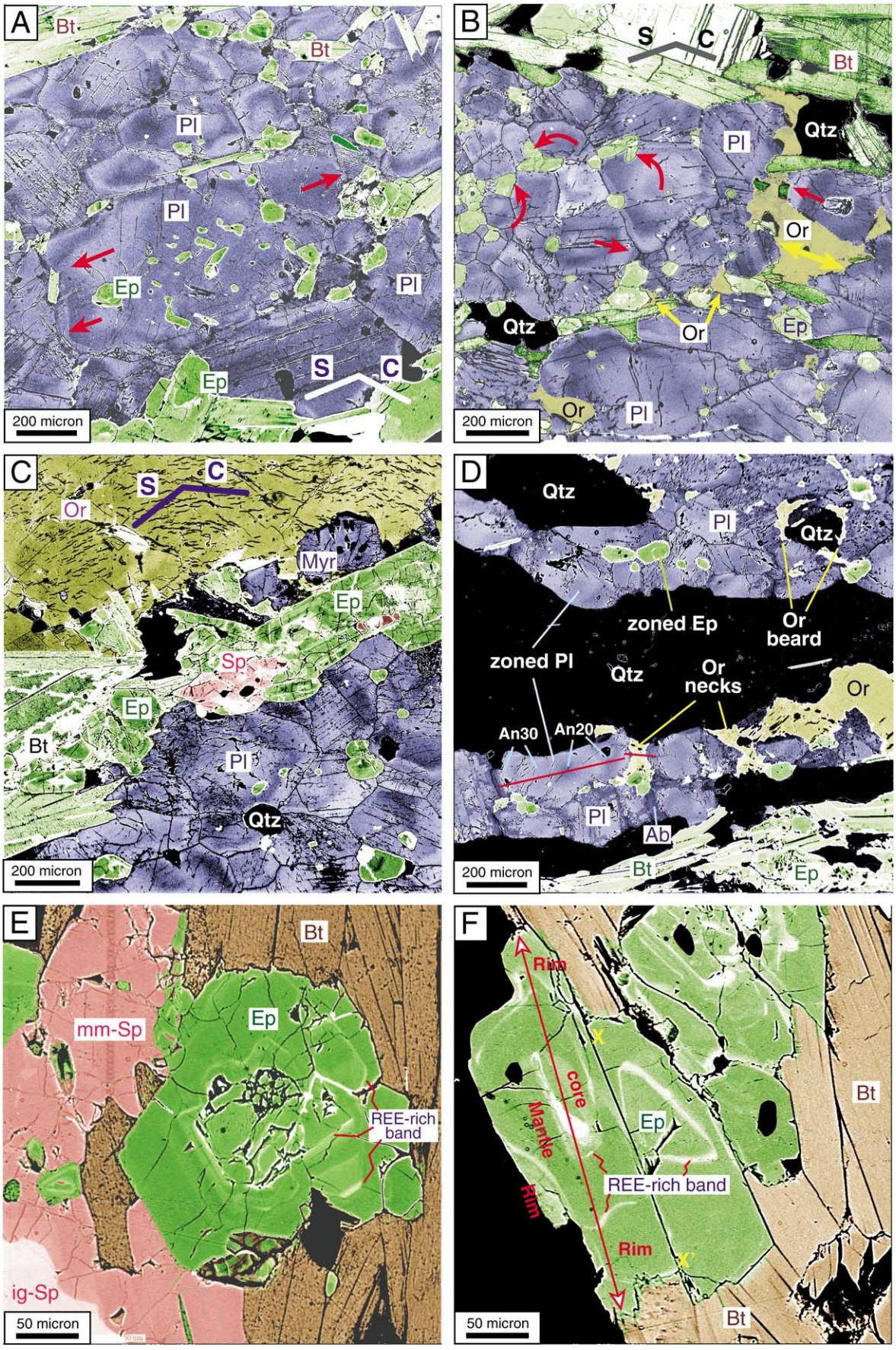
A
Bt
Bt
Pl
Pl
Ep
Pl
S
C
Ep
200 micron
B
S
C
Bt
Qtz
Pl
Or
Qtz
Or
Ep
Or
Pl
200 micron
C
S
C
Or
Myr
Ep
Sp
Ep
Bt
Pl
Qtz
200 micron
D
Qtz
Pl
Qtz
zoned Ep
Or
beard
zoned Pl
Qtz
Or
necks
Or
An30
An20
Pl
Ab
Bt
Ep
200 micron
E
Bt
mm-Sp
Ep
REE-rich
band
ig-Sp
50 micron
F
Rim
X
core
Mantle
Rim
Bt
Ep
REE-rich band
Rim
X'
Bt
50 micron

Table 1
Representative electron microprobe analysis of feldspar (n.d. = not detected, n.a. = not analyzed. Operating conditions of 15 kV, 10 nA, 5 μm beam size, and natural mineral standards in all tables except as indicated otherwise)

	Orthoclase phenocryst				Orthoclase neck		Plagioclase		
	Host	Ab exsolution[a]	Average[b]	Pl inlcusion[c]	Low Ba	High Ba	Core	Core	Rim
SiO_2	64.42	67.03	64.96	61.35	64.12	63.90	60.19	63.03	67.34
Al_2O_3	18.69	20.92	19.09	24.50	18.73	18.94	25.54	24.00	20.34
CaO	n.d.	0.99	0.08	5.97	n.d.	n.d.	6.01	4.61	1.02
FeO	n.d.	0.10	0.03	0.04	n.d.	n.d.	0.08	0.09	0.13
BaO	0.50	0.01	0.39	0.03	0.60	1.16	n.a.	n.a.	n.d.
Na_2O	0.57	10.51	1.71	8.02	0.26	0.38	7.82	8.48	10.47
K_2O	15.89	0.42	13.90	0.17	15.79	15.38	0.13	0.17	0.10
Total	100.06	99.97	100.16	100.08	99.49	99.75	99.77	100.38	99.39
	Number of ions based on eight oxygen atoms								
Si	2.98	2.94	2.98	2.72	2.98	2.97	2.68	2.77	2.96
Al	1.02	1.08	1.03	1.28	1.03	1.04	1.34	1.25	1.05
Ca	0.00	0.05	0.00	0.28	0.00	0.00	0.29	0.22	0.05
Fe	0.00	0.00	0.00	0.00	0.00	0.00	0.00	0.00	0.01
Ba	0.01	0.00	0.01	0.00	0.01	0.02	–	–	0.00
Na	0.05	0.89	0.15	0.69	0.02	0.03	0.68	0.72	0.89
K	0.94	0.02	0.82	0.01	0.94	0.91	0.01	0.01	0.01
Total	5.00	4.98	4.99	4.99	4.98	4.98	4.99	4.97	4.96

[a] > 10 μm exsolution lamellae.
[b] $n = 61$, 5 μm beam size and $n = 17$, 20 μm beam size: identical results.
[c] Inclusions of plagioclase that may be coarse exsolution lamellae.

3.7. Quartz

Quartz is not uniformly distributed in these rocks. It makes up only a small part of feldspar-rich domains, especially in regions adjacent to orthoclase porphyroblasts at grain boundaries normal to the shortening direction (Figs. 3 and 4). It is common in beards and pressure shadows around orthoclase phenocrysts, but it also defines pure quartz layers parallel to *C* (Fig. 4). Grains are typically slightly undulose and equant, 200–400 μm in diameter, with smooth interfaces with feldspars, but moderately sutured boundaries with adjacent quartz grains. Larger undulose grains up to 3–5 mm long define quartz-rich folia (Fig. 3).

4. Discussion

In the above section we have shown that virtually all metamorphic minerals in the granodioritic orthogneiss are zoned, and that the zoning patterns show elongation of the grains. In this section we bring these observations together to interpret deformational processes. First, however, we must establish which minerals are metamorphic and which are relict igneous grains.

4.1. Metamorphic petrology

4.1.1. Metamorphic versus igneous minerals

The Glastonbury gneiss complex is a large body of

Fig. 5. Colorized backscattered electron images of small regions of Glastonbury orthogneiss, colored to emphasize mineralogical and compositional differences. Colors as in Fig. 4 except in (E) and (F) where biotite is brown. Shades of dark (sodic) and pale (calcic) blue show that zoning in plagioclase is nearly universal. Dark and pale (REE-rich) green show zoning in epidote is common. (A) A typical plagioclase-rich domain, showing a relatively large plagioclase grain with overgrowths at grain boundaries that are nearly normal to the stretching direction (red arrows) in a cluster of smaller grains. (B) The selective occurrence of epidote grains at plagioclase triple junctions and penetrating plagioclase grains (curved red arrows) in a feldspar-rich layer. Overgrowths on plagioclase grains extend the dimensions parallel to (C) (straight red arrows). Orthoclase necks (yellow) between plagioclase, quartz, and epidote grains (yellow arrows) allow extension of the aggregate (see also (D)). (C) The local embayment of an orthoclase phenocryst by biotite, epidote, and myrmekite. Biotite, epidote, and sphene define the dark folia typical of Fig. 3. The curved exsolution lamellae of albite in the orthoclase, parallel to the external *S–C* fabric may reflect plastic deformation of this grain. (D) Image of quartz-rich and feldspar-rich layers, showing the occurrence of orthoclase as necks between plagioclase grains, and as beards on quartz grains. The positions of microprobe traverses of plagioclase and orthoclase (Fig. 6A and E) are indicated with the red lines. The truncation of zoning along the upper boundary of the analyzed plagioclase grain probably reflects the dissolution of the upper part of that grain. (E) An intergrowth of metamorphic sphene, biotite, and subhedral zoned epidote. Igneous core of sphene (pale pink) is visible in lower left corner. Concentric bands of REE in epidote monitor the subhedral growth of the grain. (F) An intergrowth of biotite (brown) and epidote (green) where quartz as inclusions and a layer (left) is black. REE-rich bands in the epidote (white) outline core, mantle, and rim growth stages. The truncation of these bands along grain boundary X–X′ is evidence for the dissolution of both epidotes along this boundary.

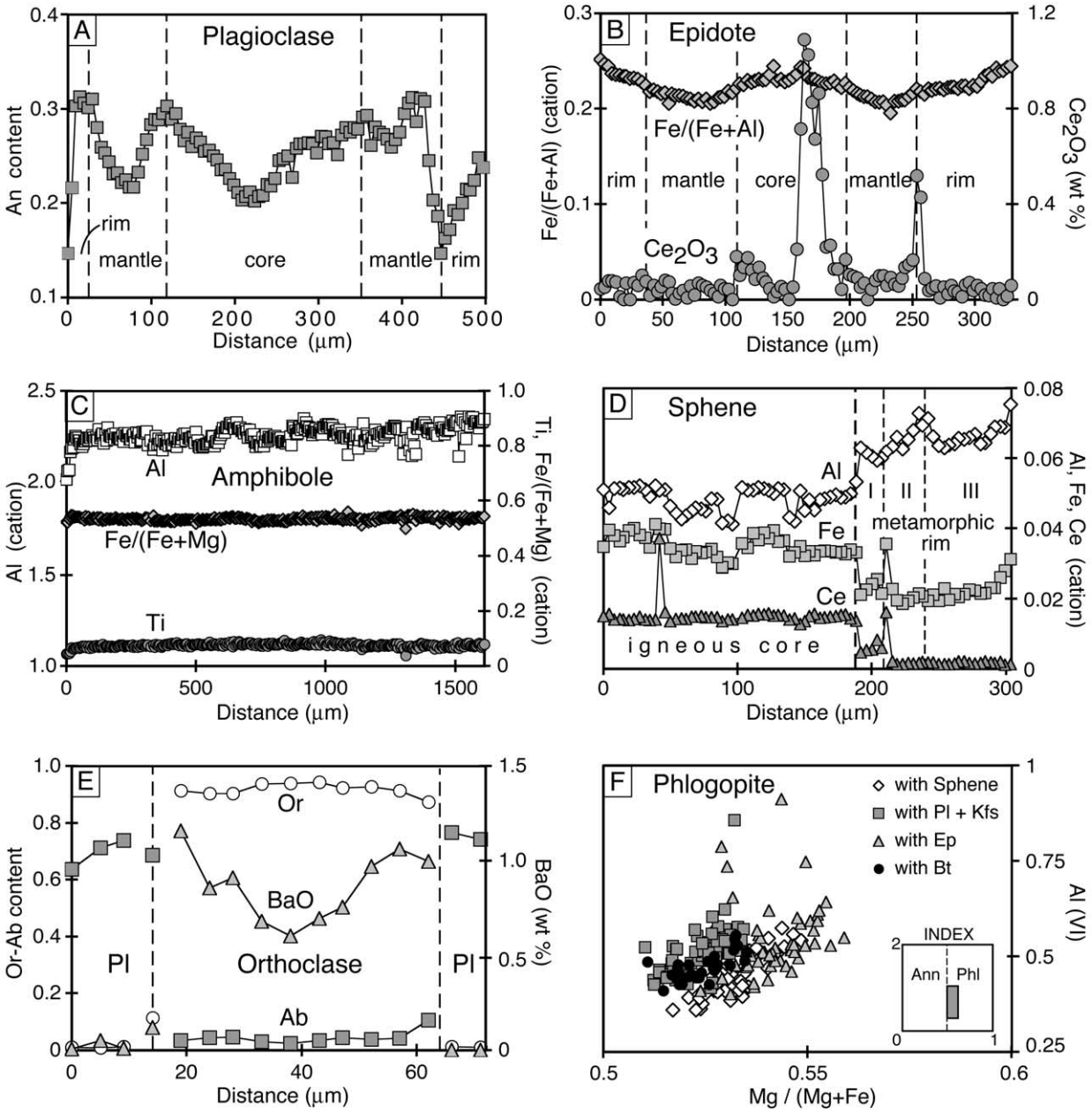

Fig. 6. Typical compositional variations of minerals in this study. (A) Compositional profile of a typical plagioclase grain, here from Fig. 5D, showing multiple overgrowths. (B) Compositional profile of the epidote grain shown in Fig. 6F. The core–mantle–rim structure is marked by increases in the concentration of Ce_2O_3 (and other REE), while the change in the Fe/Fe + Al varies continuously. (C) Compositional profiles of amphibole showing the lack of chemical zoning at the scale of >1 mm. (D) Compositional profile of sphene crossing the igneous core and metamorphic rim of the grain. Fluctuations in composition of the igneous core correlate with euhedral oscillatory zoning, while fluctuations in Fe, Al, and other trace elements define core, mantle and rim regions (I, II, III, respectively) in the metamorphic overgrowth. (E) Compositional profile of the orthoclase neck between the two plagioclase grains of Fig. 5D. The concentration of BaO in the rims of the orthoclase neck is twice that of the core, and is interpreted as growth zoning in this extensional site. The concentration of albite in the orthoclase grain is nearly constant at ~7 mol%, while it shows normal zoning in the adjacent plagioclase grains. The concentrations of Or and BaO in the plagioclase are uniformly low. (F) The compositional range of biotite solid solutions as a function of host assemblage, plotted as a function of Mg/(Mg + Fe) (atomic) and octahedral Al. Phlogopites associated with feldspars are richer in Fe and Al(VI), while those associated with biotite are richer in Mg and poor in Al(VI).

orthogneisses of variable composition. A southern phase of this complex, 15 km long and 3 km wide, contains an augen gneiss with conspicuous crystals of orthoclase with Carlsbad twins. This twinning is common in igneous rocks, and unknown to us in metamorphic rocks. The integrated composition of the grains is more much sodic than the second textural variety that is intergrown with plagioclase. These features plus the trial thermometry (Section 4.1.2) suggest that the megacrysts are phenocrysts that crystallized in the original Ordovician intrusion.

Table 2
Representative electron microprobe analysis of sphene and epidote (U, Th, Pb, Sn, La, Zr, K, Mg, Na analyzed; all <0.01 wt% oxide)

	Sphene				Epidote		
	Igneous core		Metamorphic rim		Core	Core	Rim
	High Ce	Low Ce	High Y	Low Y	High Ce	Low Ce	
SiO_2	29.38	29.14	29.18	28.60	35.64	36.27	36.45
TiO_2	36.18	35.45	35.66	35.98	0.06	0.06	0.07
P_2O_5	0.31	0.25	0.27	0.25	0.23	0.22	n.a.
Nb_2O_5	0.09	0.05	0.28	0.30	n.d.	n.d.	n.a.
Ta_2O_5	n.d.	n.d.	n.d.	n.d.	0.05	n.d.	n.a.
Al_2O_3	1.11	1.36	1.51	1.53	23.58	25.04	23.61
Fe_2O_3	1.06	1.66	0.74	0.79	10.96	10.22	12.09
Y_2O_3	0.16	0.22	0.15	0.02	0.27	0.01	0.01
Ce_2O_3	0.65	0.56	0.17	0.18	0.77	0.10	0.05
Pr_2O_3	0.18	0.18	n.d.	n.d.	0.03	0.08	n.a.
Nd_2O_3	0.03	0.13	0.02	0.03	0.09	0.03	0.00
Sm_2O_3	n.d.	0.04	n.d.	0.02	0.01	n.d.	n.a.
Gd_2O_3	0.05	0.14	n.d.	n.d.	0.11	0.05	n.a.
Dy_2O_3	n.d.	n.d.	n.d.	n.d.	0.09	n.d.	n.a.
Yb_2O_3	0.09	n.d.	n.d.	0.03	0.01	0.03	n.a.
MnO	0.17	0.14	0.10	0.10	0.30	0.28	0.35
CaO	27.63	27.80	27.98	27.94	21.14	22.49	22.54
F	0.31	0.49	0.38	0.50	0.09	0.11	0.10
O = F	− 0.13	− 0.21	− 0.16	− 0.21	− 0.04	− 0.05	− 0.04
Total	97.41	97.46	96.34	96.38	93.63	94.94	95.23
	Number of ions based on 5 oxygen atoms for sphene and 25 for epidote						
Si	0.991	0.985	0.991	0.975	5.939	5.901	5.954
Ti	0.918	0.901	0.911	0.922	0.007	0.007	0.009
P	0.009	0.007	0.008	0.007	0.033	0.030	–
Nb	0.001	0.001	0.004	0.005	–	–	–
Ta	–	–	–	–	0.002	–	–
Al	0.044	0.054	0.060	0.061	4.630	4.802	4.544
Fe	0.027	0.042	0.019	0.020	1.375	1.252	1.486
Ca	0.999	1.007	1.018	1.020	3.775	3.920	3.945
Mn	0.005	0.004	0.003	0.003	0.042	0.039	0.048
Y	0.003	0.004	0.003	–	0.024	0.001	0.001
Ce	0.008	0.007	0.002	0.002	0.047	0.006	0.003
Pr	0.002	0.002	–	–	0.002	0.005	–
Nd	–	0.002	–	–	0.005	0.002	–
Sm	–	–	–	–	–	–	–
Gd	0.001	0.002	–	–	0.006	0.003	–
Dy	–	–	–	–	0.005	–	–
Yb	0.001	–	–	–	–	0.002	–
F	0.033	0.053	0.041	0.054	0.046	0.056	0.050
Total cations	3.009	3.017	3.019	3.015	15.895	15.967	15.991

Matrix feldspars are probably all metamorphic. Plagioclase never shows albite twinning nor the oscillatory zoning typical of igneous rocks. The lack of twinning together with its coarse-scale, fluctuating zoning, inclusions of epidote and biotite, and participation in the metamorphic layering (Figs. 3–5) indicates that the plagioclase is metamorphic. Orthoclase is intergrown with this plagioclase. It also occurs as beards on orthoclase phenocrysts, and as beards and necks on metamorphic plagioclase and epidote grains in the feldspar domains. Some grains even show zoning in BaO content that correlates with the microstructure (Fig. 6E). Thus both orthoclase and plagioclase crystallized in feldspar-rich domains during the development of the foliation.

Magnesiohastingsite is probably also magmatic. Its composition (Table 3) cannot be used to discriminate between crystallization at high-grade metamorphic and igneous conditions. However, unlike many metamorphic amphiboles, it is only weakly zoned, and this at the scale of 2 mm (Fig. 6C), and trial thermometry (Section 4.1.2) is not consistent with the epidote–amphibolite facies conditions of metamorphism.

Beyond orthoclase phenocrysts and amphibole, the cores of sphenes and zircons, both dated as Ordovician by U–Pb

Table 3
Representative electron microprobe analysis of amphibole and biotite

	Amphibole[a]		Biotite[b]		
	Core	Rim	With sphene	With feldspar	With epidote
SiO_2	42.06	43.08	36.32	36.39	37.15
TiO_2	0.68	0.57	1.34	1.86	2.35
Al_2O_3	11.81	11.70	15.81	16.23	16.84
FeO	18.19	18.42	19.84	18.62	17.30
MnO	0.68	0.57	0.36	0.48	0.35
MgO	9.26	9.47	12.07	11.50	11.42
CaO	11.01	11.01	n.d.	n.d.	n.d.
Na_2O	1.28	1.35	0.05	0.09	0.05
K_2O	1.42	1.29	9.19	9.71	9.47
F	0.23	0.26	0.41	0.38	0.34
O = F	− 0.10	− 0.11	− 0.17	− 0.16	− 0.14
Total	96.52	97.60	95.21	95.09	95.11
	Number of ions based on 23 oxygen atoms for amphibole and 22 for biotite				
Si	6.38	6.44	5.55	5.55	5.60
Ti	0.08	0.06	0.15	0.21	0.27
Al	2.11	2.06	2.85	2.92	2.99
Fe^{3+}	0.67	0.64	–	–	–
Fe^{2+}	1.64	1.66	2.53	2.37	2.18
Mn	0.09	0.07	0.05	0.06	0.04
Mg	2.09	2.11	2.75	2.61	2.57
Ca	1.79	1.77	0.00	0.00	0.00
Na	0.38	0.39	0.01	0.03	0.01
K	0.28	0.25	1.79	1.89	1.82
F	0.11	0.12	0.20	0.18	0.16
Total	15.62	15.57	15.68	15.65	15.48

[a] Ferric iron of amphibole calculated following Holland and Blundy (1994) yield near maximun Fe^{3+} estimates and a magnesiohastingsite classification of Leake et al. (1997).
[b] Ba analyzed; all <0.01 wt% oxide. All iron treated as FeO.

methods (Aleinikoff et al., 2001) are the only other minerals of reliably igneous origin. The other minerals are all metamorphic. Permian U–Pb SHRIMP ages (Aleinikoff et al., 2001) of sphene overgrowths on igneous sphene (Figs. 4 and 5E) are relatively high in Al and F, consistent with the compositions of metamorphic sphenes (Kowallis et al., 1997). Biotite and epidote are intergrown with metamorphic sphene (Figs. 4 and 5C and E), and together define the metamorphic foliation. The composition of biotite is sensitive to the local metamorphic mineral assemblage (Fig. 6F), and must have grown at the same time. Quartz forms pressure shadows around orthoclase phenocrysts (Fig. 3) and participates in defining the metamorphic foliation (Figs. 3 and 4), so it is also metamorphic in origin.

4.1.2. Igneous crystallization conditions

In principle the conditions of igneous crystallization can be estimated from the compositions of igneous minerals. Although igneous grains are present in these rocks, there is abundant evidence in mineral textures and assemblages for the very poor preservation of igneous chemical equilibrium. For example, orthoclase textures are complicated, probably by exsolution and deformation but have an integrated composition of ~Or82. Trial feldspar thermometry (Elkins and Groves, 1990) with a plagioclase of An40 and 5 kb pressure gives 670–720°C, consistent with igneous crystallization temperatures, but not with epidote–amphibolite facies metamorphic conditions. Exploratory hornblende–plagioclase thermometry (Holland and Blundy, 1994) gives a similar temperature of ~700°C.

The amphibole Al barometer is tempting to apply, but the buffer assemblage is incomplete: no Fe–Ti oxide is present. If one had been present in the igneous rock, the pressure estimated would be between 5.5 (Johnson and Rutherford, 1989) and 7 kb (Schmidt, 1992). These P–T conditions are consistent with near solidus magmatic crystallization conditions (Schmidt, 1993), and support the above conclusions that the orthoclase and amphibole are relict igneous minerals.

4.1.3. Metamorphic crystallization conditions

The high variance of the metamorphic assemblage and the poor approach to chemical equilibrium among the zoned metamorphic minerals in these rocks preclude rigorous thermobarometric calculations. However, estimates can be made if local equilibrium between adjacent grains is assumed. For example, the rim compositions of orthoclase and plagioclase in feldspar domains may closely approach equilibrium. Using the thermometer of Elkins and Groves (1990) and the compositions of coexisting feldspars from regions like those shown in Fig. 5B and D yield nearly pressure-independent temperatures of ~425°C; this is probably a minimum estimate considering the undeformed state and likely late stage of development of these microstructures. Another minimum estimate comes from reset $^{40}Ar/^{39}Ar$ (Permian) amphibole ages that reflect at least epidote–amphibolite facies metamorphic conditions in the Alleghanian (Wintsch et al., 1998) or temperatures of $> \sim 500$°C (McDougall and Harrison, 1988). Model P–T–t paths similar to Wintsch et al. (1993) suggest peak temperatures of ~600°C at 6 kb. This is consistent with the staurolite–kyanite grade assemblages just east of these rocks (e.g. Snyder, 1970; Hickey and Bell, 1999). Finally the assemblages of reaction 1 are typical of the epidote–amphibolite facies of metamorphism (Spear, 1993). These observations converge to yield an estimate of metamorphic conditions of these rocks of 500–600°C and 4–6 kb, as shown in Fig. 7.

4.2. Origin of foliation

4.2.1. Reaction softening

From the above analysis, it is clear that a relict igneous assemblage including orthoclase (~Or82) and magnesiohastingsite was being converted to two metamorphic assemblages: (1) Or93 + epidote + biotite + plagioclase + quartz, and (2) magnesiohastingsite + biotite + epidote + quartz + plagioclase. Although magnesiohastingsite and

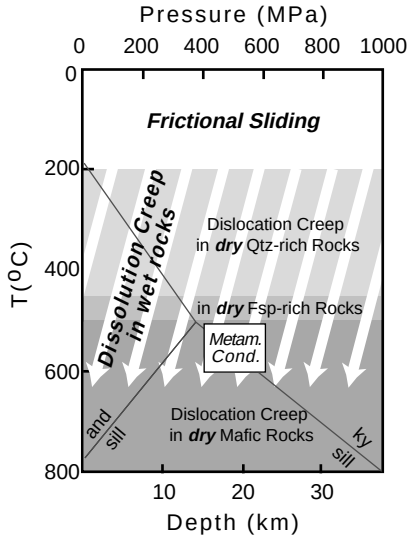

Fig. 7. Deformation mechanisms as a function of temperature, based on the strength envelopes extrapolated from experimental data and geothermal gradient of Kohlstedt et al. (1995) and Rybacki and Dresen (2000) from Fig. 1. The diagram shows the regions of frictional sliding below 200°C (white), dislocation creep in dry quartz-rich rocks (pale gray), in dry feldspar-rich rocks (medium gray), and dry mafic rocks (dark gray) with increasing temperature. The diagram thus predicts dislocation creep in all dry quartzo–feldspathic rocks at temperatures above 450°C. However, the operation of *dissolution* creep at the epidote–amphibolite facies conditions of the rocks described here (box) extends the field of operation of this deformation mechanism to these temperatures (white diagonal lines). Aluminosilicate triple point from Holdaway and Mukhopadhyay (1993).

Or93 are both stable at the epidote–amphibolite facies of these rocks, they do not occur in contact. Rather, they are always separated by biotite and epidote or by quartz. Biotite and especially epidote embay, and apparently replace magnesiohastingsite (Fig. 4). Biotite intergrown with epidote also embays, and apparently replaces Or94 (Fig. 5C). These relationships reflect the incompatibility of amphibole + orthoclase via the reaction:

$$\text{magnesiohastingsite} + \text{orthoclase} = \text{biotite} + \text{epidote} \quad (1)$$

Using simplified analyses from Tables 1–3, the balanced reaction is:

$$\begin{aligned} &56KAlSi_3O_8 + 52Ca_2((Mg,Fe)_{3.5}Fe^{3+}_{0.46}Al_{1.04}) \\ &\quad [Si_{6.5}Al_{1.5}]O_{22}(OH)_2 + 30H_2O + 7O_2 \\ &= 56K((Mg,Fe)_{2.75}Al_{0.25})[Si_{2.75}Al_{1.25}]O_{10}(OH)_2 \\ &\quad + 52Ca_2FeAl_2Si_3O_{12}(OH) + 196SiO_2 \end{aligned} \quad (2)$$

This is a discontinuous reaction reflecting the incompatibility of magnesiohastingsite + orthoclase under temperatures considerably less than those of the original igneous crystallization (Fig. 7). This reaction explains well the intergrowth of biotite and epidote that defines the S–*C* fabric, and the apparent replacement relationships of these minerals against magnesiohastingsite and orthoclase. It is significant that quartz is not texturally associated with the other reaction products. It is likely that its relatively high solubility frees it to precipitate in its own layer, as shown in Figs. 3–5D. Some of the quartz must have moved at least 5 mm, presumably as aqueous silica, but local quartz veins up to 20 cm long suggest that some silica moved several decimeters of more.

4.2.2. Growth during extension: dissolution-precipitation creep

The concentration of biotite, quartz, and plagioclase into folia parallel to the *C* foliation (Fig. 4) produces a highly layered rock in which different deformation mechanisms may dominate in each layer. Biotite and quartz can deform relatively easily by dislocation creep. However, the pervasive chemical zoning and especially truncated zoning of the other minerals suggest that they did not deform by dislocation creep.

Many grains display overgrowths around relatively equant cores. Zoning in plagioclase is universal (Figs. 4 and 5), and core regions of plagioclase grains commonly show up to three stages of growth and overgrowth (Fig. 6A). In microstructures where the precipitation of plagioclase did not keep pace with extension, orthoclase (~Or92) precipitated as beards and necks (Figs. 4 and 5B and C).

The epidote–sphene overgrowth pair is an interesting coupled reaction. Epidote grains, especially those intergrown with biotite appear as overgrowths on relatively equant cores. Stages of overgrowth of epidote are marked by 30–50-μm-wide rings of epidote enriched in REEs and Y (Table 2). The only local source for REEs is the igneous sphene. Thus, pulses of extension in the rock, which localize dissolution and overgrowth in epidote, also lead to pulses of dissolution of igneous sphene and precipitation of metamorphic sphene. Because the metamorphic sphene accepts only about a third of the REEs in solid solution that igneous sphene does (Table 2), the REEs released by the dissolution of igneous sphene are concentrated into metamorphic epidote. At the same time, the pulses of overgrowth of metamorphic sphene are documented by the fluctuating but increasing Al concentrations (Fig. 6D). Thus we surmise that the three stages of growth recognized in plagioclase are also present in epidote and sphene.

While the evidence for precipitation in the form of overgrowths is abundant in these rocks, evidence for dissolution is less common but still present in the form of truncated zoning. Zoning in plagioclase is commonly truncated but in some textures it is difficult to prove that this is not due to incomplete crystallization. The case with epidote is more compelling. Fig. 5F shows a cluster of epidote grains (green) in a biotite-rich (brown) layer. The two grains on the left show the REE-rich bands (white) typical of most epidote grains. The biotite host formed one of the weakest aggregates in this rock (Shea and Kronenberg, 1993) and probably deformed by dislocation creep. The smooth zoning

in the epidote grains shows no substantial flow in these grains, and slip seems to have been localized along the epidote–epidote surface (X–X′, Fig. 5F). Here the truncation of the REE bands provides strong evidence for the dissolution of both epidote grains along this unusually straight boundary. Evidence for elongation comes from the asymmetric overgrowths on the longer grain (red arrows). Thus evidence for dissolution as well as precipitation in these rocks is strong, and much of the strain in these rocks can be attributed to processes involving dissolution and precipitation.

4.2.3. Replacement creep

Several reactions occur in those rocks that indicate that flow occurs, in part, by mass transport, and that volumetric strains are non-zero. Reaction 1 above, while producing phases of lower intrinsic strength and thus leading to reaction softening, constitutes a volume reduction. As such its operation will contribute to the shortening of the rock perpendicular to the *S* surfaces. Moreover, the redistribution of the quartz makes the shortening effect even greater (up to 27%). Using representative molar volumes, the change in volume for reaction 1, ignoring gases, is −3.5%. It is driven to the right by an increase in fO_2, fH_2O, and pressure. The reaction produces approximately equal volumes of biotite and epidote, and is significant in that some of the weakest minerals in metamorphic rocks, biotite, and quartz replace some of the stronger, feldspar and especially hornblende. The segregation of these weak minerals into layers rich in biotite or quartz contributes greatly to the overall weakening of the rock (Shea and Kronenberg, 1993), especially considering the likely random orientation of grains and interlocking textures in the igneous protolith.

Another reaction causing a significant volume reduction is the replacement of orthoclase by the myrmekitic intergrowth of quartz and plagioclase (Figs. 3 and 5C):

$$1.25\text{orthoclase} + 0.25Ca^{++} + 0.75Na^{+} = \text{plagioclase(An25)} + 1.25K^{+} \quad (3)$$

The change in volume of the solids for this reaction is $-15\ cm^3/mol$ of plagioclase, corresponding to an 11% volume reduction. In these rocks, as in those described by Simpson and Wintsch (1989), myrmekite is also concentrated at interfaces that are perpendicular to the shortening direction (Fig. 4).

It also appears that epidote replaced only plagioclase in some plagioclase domains. Many epidote grains embay plagioclase and truncate plagioclase zoning, especially at interfaces parallel to the foliation (red arrows, Fig. 5B). In contrast, orthoclase + quartz fill spaces between grains at interfaces normal to the foliation. Where truncation by epidote is most conspicuous (e.g. Fig. 5B), only plagioclase and epidote are involved. Simplifying the formula to minimize the calculated volume loss, the reaction is:

$$8\text{Plag(An25)} + 8Ca^{++} + 15H_2O + 5Fe^{+3} = 5\text{epidote} + 6Na^{+} + 7SiO_2 + 25H^{+} \quad (4)$$

with a 17% volume loss, in addition to the release of silica. This silica could easily fill the extension sites in Fig. 5, or react with aqueous K^+ to produce necks of Or90.

4.2.4. Reaction mechanisms

Carmichael (1969) identified the local metasomatism that accompanied reactions in pelitic rocks, and noted that in general the aqueous ionic reactants and products of these reactions balance, such that rocks behave as closed chemical systems (centimeter scale) except for volatiles. The typical igneous compositions of these granodioritic rocks (Leo et al., 1984) suggests that this is the case here as well. The metastability of the orthoclase + magnesiohastingsite assemblage probably contributed greatly to the dissolution of both the orthoclase and the magnesiohastingsite phenocrysts. The K^+ liberated by the dissolution of orthoclase reacted with magnesiohastingsite to produce biotite. This liberated Ca^{++} and some Na^+. The Ca^{++} reacted with the amphibole and plagioclase to produce epidote. Most of these reactions constitute a volume loss, and so would have been driven by a relatively high normal stress perpendicular to the *S* fabric. The same high normal stress would have increased the dislocation density in weaker minerals at strong–weak mineral interfaces, and this strain energy would have further driven these dissolution reactions (Wintsch, 1985). The ultimate distribution of reaction products was controlled in part by normal stress producing the composite foliation and by extension parallel to it.

5. Conceptual model of fabric development

The texture of the protolith of the augen gneiss is not available, but it was undoubtedly granodioritic porphyry. Under epidote–amphibolite facies conditions of metamorphism, the orthoclase phenocrysts reacted with relict magnesiohastingsite to produce biotite, epidote, and quartz. The differential mobility of K^+ and SiO_2 led to the transport of K^+ from the dissolving orthoclase (Or82) to the reacting magnesiohastingsite. The product biotite defined a new *C*-foliation, and the strong preferred orientation and contiguity of these biotite grains is interpreted to have facilitated dislocation creep under the applied stress in these new folia. Because none of the other minerals in the rock could flow by dislocation creep as fast as biotite, many microextensional sites were produced. SiO_2 and K^+ were drawn to these sites, producing quartz and orthoclase beards on phenocrysts and on extending plagioclase grains. Where quartz layers developed, deformation may also have occurred by dislocation creep. In this particular example,

the common occurrence of two overgrowths on cores of plagioclase, epidote, and sphene shows that at least three pulses of extension occurred.

6. Dissolution and precipitation creep

With the extrapolation of experimental rheological studies to the slower strain rates of natural crustal rocks, the depth domains of frictional sliding and dislocation creep in dry crust have been predicted. The yield strengths in the brittle field are a strong function of confining pressure (e.g. Kohlstedt et al., 1995), but deformation by dislocation creep is thought to be more sensitive to temperature, strain rate, and the fugacity of H_2O rather than to confining pressure (Rybacki and Dresen, 2000). These extrapolations to a strain rate of 10^{-14} have predicted that in quartz-rich rocks, brittle deformation dominated by fracture mechanisms gives way to ductile deformation by dislocation creep at about 200°C (Fig. 1). This brittle-ductile transition occurs at higher temperatures in rocks containing minerals in which dislocation migration mechanisms are not activated until higher temperature. Plasticity is activated in plagioclase at ~450°C (Rybacki and Dresen, 2000), while plasticity in clinopyroxene, one of the strongest rock-forming minerals at crustal conditions, is not predicted until >500°C (Fig. 1). If the presence of H_2O is considered, then the frictional limits drop to lower differential stresses (Chester, 1995; Kohlstedt et al., 1995) and a field of 'pressure-solution' displaces dislocation creep in the temperature range of 200 to at least 300°C (Snoke et al., 1998).

To place the strength information of Fig. 1 in more petrologic terms, we transfer it to the pressure–temperature diagram of Fig. 7. Here the P–T conditions of the Glastonbury orthogneiss (Section 4.1.3) lie well within the dislocation creep fields of quartz and feldspar, as extrapolated from dry experimental studies. However, this extrapolation may not be valid where fluids are present during deformation. Fluids were present in the Glastonbury gneiss as demonstrated by the operation of reaction 1, which requires the introduction of H_2O and O_2. Indeed, most minerals in these rocks deformed primarily by dissolution-precipitation processes that require the presence of an aqueous solution to accommodate the local mass transfer. Thus the dissolution-precipitation creep field in wet rocks must extend at least to the temperatures (and depths) of the Glastonbury gneiss (Fig. 7). The significance of these results may lie in the recognition that at relatively high metamorphic grades dissolution-precipitation processes are activated at lower stresses than is dislocation creep (see also Stoeckert et al., 1999). If this is true, then the strength of the crust estimated from dry experiments may produce a maximum estimate of crustal strength, while consideration of fluid-assisted deformation mechanisms may give more realistic estimates (e.g. Chester, 1995).

7. Driving mechanism

The excess energy driving mineral dissolution may come from three sources: inhomogeneous stress, recoverable elastic strain energy, and permanent 'plastic' strain energy associated with dislocation and twin boundaries (Wintsch, 1985). We have been an advocate of the latter plastic strain as a source of energy driving dissolution (Wintsch and Dunning, 1985), particularly in feldspars (Knipe and Wintsch, 1985; Wintsch and Andrews, 1988; Simpson and Wintsch, 1989). This is also probably the case here, as the density of deformation twins and undulosity in orthoclase tends to be higher in regions adjacent to plagioclase (myrmekite) and epidote replacements. However, because the sites of high normal stress are also the sites of high dislocation density, these thermodynamically distinct sources of energy should lead to dissolution at the same sites, and without specific textural evidence (Bosworth, 1981; Engelder, 1982), they cannot be discriminated. However, the commonly negative volume changes for the reactions identified above points toward stress as a component of the driving force for dissolution.

Whatever the specific source of excess internal energy, this energy rendered the strained regions of those grains metastable. In the absence of fluids this energy would drive recovery and recrystallization processes (e.g. Passchier and Trouw, 1996). However, with fluids present, the dissolution of grains or parts of grains with high normal stresses or with high internal energy was more easily activated than dislocation creep, and dissolution and replacement creep became the dominant deformation mechanism. Excess internal energy increased the solubility of the deformed regions of grains (Wintsch and Dunning, 1985) and drove a complicated series of dissolution reactions similar to those caused by the metastability of the magnesiohastingsite + orthoclase. Because the dissolution occurred selectively at sites of high normal stress, it contributed to changing the shapes of the grains. Where dissolution and precipitation occur at the same site, volume-loss replacements occurred. Where precipitation of the dissolved components produced beards and overgrowths, the rock extended in the stretching direction. The overgrowths appear to be undeformed, and the precipitation of minerals in extensional sites probably limited the rate of extension, similar to displacement-controlled fibre growth (Passchier and Trouw, 1996).

8. Conclusions

We have found abundant evidence for overgrowth of orthoclase, plagioclase, epidote, and sphene leading to elongation in the extension direction in a developing S–C fabric in an orthogneiss. There is strong evidence for dissolution of igneous orthoclase and amphibole and metamorphic epidote on surfaces facing the shortening direction. There is also evidence for the replacement of orthoclase and

plagioclase by biotite and epidote. These features lead to the conclusion that under epidote–amphibolite facies conditions, creep in these rocks was accomplished by dissolution-precipitation, reaction, and replacement processes. Some dislocation creep at these conditions undoubtedly occurred in evolving biotite folia and quartz layers, but the bulk strain in the large volume percentage of the rock appears to have occurred mostly by chemical process and mass transfer, even if these chemical processes were mechanically driven. It is important to note that relict igneous minerals remain, and all metamorphic minerals are zoned, so that even at these epidote–amphibolite facies conditions, chemical equilibrium among the metamorphic minerals has not occurred. Estimates of the strength of wet crust that disregard these solution transfer processes are thus likely to be too high.

Acknowledgements

This work has benefited from discussions with J. Aleinikoff, T. Bell, T. Byrne, M. Coleman, D.M. Carmichael, G. Hirth, S. Johnson and M. Kunk. We especially thank Mike Williams for editorial handling, and B. Bayly and A. Kronenberg for very thorough reviews of an earlier draft. K. Yi was partially supported by the BK21 project of the Korean government. The study was partially supported by NSF grants EAR-9418203 and EAR-9909410 to Wintsch.

References

Aleinikoff, J.N., Wintsch, R.P., Fanning, C.M., Dorais, M.J., 2002. U–Pb Geochronology of complexly zoned sphene: an integrated SEM, EMPA, and SHRIMP study. Chemical Geology, Isotope Science Section, in press.

Blatt, H., 1992. Sedimentary Petrology. W.H. Freeman, New York.

Bosworth, W., 1981. Strain enhanced dissolution of halite. Tectonophysics 78, 509–525.

Carmichael, D.M., 1969. On the mechanism of prograde metamorphic reactions in quartz bearing pelitic rocks. Contributions to Mineralogy and Petrology 20, 244–267.

Chester, F.M., 1995. A rheological model for wet crust applied to strike-slip faults. Journal of Geophysical Research 100, 13033–13044.

Coleman, M., Pulver, M., Byrne, T., Kiyokawa, S., Wintsch, R., Davidek, K.K., Martin, M., 1997. Late Paleozoic shortening and metamorphism within the Bronson Hill terrane, central Connecticut. Geological Society of America Abstracts with Programs 29, A231.

Elkins, L.T., Groves, T.L., 1990. Ternary feldspar experiments and thermodynamic models. American Mineralogist 75, 544–559.

Engelder, T., 1982. A natural example of the simultaneous operation of free face dissolution and pressure solution. Geochimica et Cosmochimica Acta 46, 69–74.

Harrison, T.M., Spear, F.S., Heizler, M.T., 1989. Geochronologic studies in central New England II: Post-Acadian hinged and differential uplift. Geology 17, 185–189.

Hickey, K.A., Bell, T.H., 1999. Behavior of rigid objects during deformation and metamorphism: a test using schists from the Bolton syncline, Connecticut, USA. Journal of Metamorphic Geology 17, 211–228.

Holdaway, M.J., Mukhopadhyay, B., 1993. A reevaluation of the stability relations of andalusite: thermochemical data and phase diagram for the aluminum silicates. American Mineralogist 78, 298–315.

Holland, T., Blundy, J., 1994. Non-ideal interactions in calcic amphiboles and their bearing on amphibole–plagioclase thermometry. Contributions to Mineralogy and Petrology 116, 433–447.

Johnson, M.C., Rutherford, M.J., 1989. Experimental calibration of the aluminum-in-hornblende geobarometer with application to Long Valley caldera (California) volcanic rocks. Geology 17, 837–841.

Knipe, R.J., Wintsch, R.P., 1985. Heterogeneous deformation, foliation development and metamorphic processes in a polyphase mylonite. In: Thompson, A.B., Rubie, D.C. (Eds.). Advances in Physical Geochemistry, vol. IV. Springer, New York, pp. 180–210 Chapter 7.

Kohlstedt, D.L., Evans, B., Mackwell, S.J., 1995. Strength of the lithosphere: constraints imposed by laboratory experiments. Journal of Geophysical Research 100, 17587–17602.

Kowallis, B.J., Christiansen, E.H., Griffen, D.T., 1997. Compositional variations in titanite. Geological Society of America Abstracts with Programs 29 (6), 402.

Leake, B.L., Woolley, A.R., et al., 1997. Nomenclature of Amphiboles: report of the subcommittee on amphiboles of the international mineralogical association, commission on new minerals and mineral names. American Mineralogist 82, 1019–1037.

Leo, G.W., Zartman, R.E., Brookins, D.G., 1984. Glastonbury gneiss and mantling rocks (a modified Oliverian dome) in south-central Massachusetts and north central Connecticut: geochemistry, petrogenesis, and radiometric age. U.S. Geological Survey Professional Paper 1295, 45.

McDougall, I., Harrison, T.M., 1988. Geochronology and Thermochronology by the $^{40}Ar/^{39}Ar$ Method. Oxford University Press, New York.

Mosher, S., 1976. Pressure solution as a deformation mechanism in Pennsylvanian conglomerates from Rhode Island. Journal of Geology 84, 355–364.

Passchier, C.W., Trouw, R.A.J., 1996. Microtectonics. Springer, New York.

Rybacki, E., Dresen, G., 2000. Dislocation and diffusion creep of synthetic anorthite aggregates. Journal of Geophysical Research 105, 26017–26036.

Schmidt, M.W., 1992. Amphibole compositions in tonalite as a function of pressure: an experimental calibration of the aluminum-in-hornblende barometer. Contributions to Mineralogy and Petrology 110, 304–310.

Schmidt, M.W., 1993. Phase relations and compositions in tonalite as a function of pressure: an experimental study at 650°C. American Journal of Science 293, 1011–1060.

Shea Jr, W.T., Kronenberg, A.K., 1993. Strength and anisotropy of foliated rocks with varied mica contents. Journal of Structural Geology 15, 1097–1121.

Simpson, C., Wintsch, R.P., 1989. Evidence for deformation induced K-feldspar replacement by myrmekite. Journal of Metamorphic Geology 7, 261–275.

Snoke, A.W., Tullis, J., Todd, V.R., 1998. Fault-related Rocks: A Photographic Atlas. Princeton University Press, Princeton, NJ.

Snyder, G.L., 1970. Bedrock geology of the Marlborough quadrangle: U.S. Geologic Survey Geologic Quadrangle Map GQ-791.

Spear, F.S., 1993, Metamorphic Phase Equilibria and Pressure-Temperature-Time Paths. Mineralogical Society of America, Monograph, 799 p.

Stoeckert, B., Wachmann, M., Kuster, M., Bimmermann, S., 1999. Low effective viscosity during high pressure metamorphism due to dissolution precipitation creep: the record of HP–LT metamorphic carbonates and siliciclastic rocks from Crete. Tectonophysics 303, 299–319.

Tucker, R.D., Robinson, P., 1990. Age and setting of the Bronson Hill magmatic arc: a reevaluation based on U–Pb zircon ages in southern New England. Geological Society of America Bulletin 102, 1404–1419.

Williams, M.I., Jercinovic, M.J., Perry, M.P., 1999. Age mapping and dating of monazite on the electron microprobe: deconvoluting multistage tectonic histories. Geology 27, 1023–1026.

Wintsch, R.P., 1985. The possible effects of deformation on chemical processes in metamorphic fault zones. In: Thompson, A.B., Rubie, D.C. (Eds.). Advances in Physical Geochemistry, vol. IV. Springer, New York, pp. 251–268 Chapter 10.

Wintsch, R.P., Knipe, R.J., 1983. Growth of a zoned plagioclase porphyroblast in a mylonite. Geology 11, 360363.

Wintsch, R.P., Dunning, J.D., 1985. The effect of dislocation density on the aqueous solubility of quartz and some geologic implications: a theoretical approach. Journal of Geophysical Research 90, 3649–3657.

Wintsch, R.P., Andrews, M.S., 1988. Deformation induced growth of sillimanite: "Stress" minerals revisited. Journal of Geology 96, 143–161.

Wintsch, R.P., Kvale, C.M., Kisch, H.J., 1991. Open system, constant volume development of slaty cleavage, and strain induced replacement reactions in the Martinsburg Formation, Lehigh Gap, PA. Geological Society of America Bulletin 103, 916–927.

Wintsch, R.P., Sutter, J.F., Kunk, M.J., Aleinikoff, J.N., Boyd, J.L., 1993. Alleghanian assembly of Proterozoic and Paleozoic lithotectonic terranes in south central New England: new constraints from geochronology and petrology. In: Cheney, J.T., Hepburn, T.C. (Eds.). Field Trip Guidebook for the Northeastern United States: 1993, GSA Annual Meeting, Boston, vol. 1, pp. H1–30.

Wintsch, R.P., Coleman, M., Pulver, M., Byrne, T., Aleinikoff, J.N., Kunk, M.J., Roden-Tice, M., 1998. Late Paleozoic deformation, metamorphic, and exhumation in central Connecticut. New England Intercollegiate Geological Conference, University of Rhode Island, Trip C2, pp. 1–25.

Wintsch, R.P., Aleinikoff, J.N., Dorais, M.J., Fanning, C.M., 1999. Electron microprobe and SHRIMP analysis of composition- and age-zoning in sphene: a record of multiple magmatic and tectonic events. Geological Society of America Abstracts with Programs 31, A80.

Wright, T.O., Platt, L.B., 1982. Pressure solution and cleavage in the Martinsburg shale. American Journal of Science 282, 122–135.

Zartman, R.E., Leo, G.W., 1985. New radiometric ages on Oliverian core gneisses, New Hampshire and Massachusetts. American Journal of Science 285, 267–280.